MADRID
inter.noise 2019
June 16 - 19
NOISE CONTROL FOR A BETTER ENVIRONMENT

Modelling of DBD plasma actuator for controlling noise from a tandem cylinders configuration

Wasala, Sahan[1]; Peng, Shia-Hui; Davidson, Lars
Division of Fluid Dynamic, Dept. of Mechanics and Maritime Science
Chalmers University of Technology, Gothenburg 41296, Sweden

González-Gutiérrez[2], Leo; Morán-Guerrero, Amadeo
Canal de Ensayos Hidrodinámicos, Escuela de Ingenieros Navales
Universidad Politécnica de Madrid (UPM), Madrid 28040, Spain

ABSTRACT

Aeroacoustic noise, generated by aircraft landing gears during the take-off or landing manoeuvres, is considered excessive, causing environmental concerns for the people living close to airports. Therefore, there is an increasing need to innovate new technologies to reduce landing gear noise. For noise reduction, it is primarily important to understand the mechanism of flow-induced landing-gear noise generation and, further, to adapt relevant new technologies to the system in order to reduce noise levels by means of effective manipulation of related aerodynamic flow features. Dielectric Barrier Discharge (DBD) plasma actuators have shown efficiency to control flow separation from bluff bodies, consequently, mitigating subsequent vortex motions and noise generation. In the present paper, a simplified landing-gear model represented by a tandem-cylinders configuration has been used. The airflow has been simulated using hybrid RANS/LES. Effects of the plasma actuation are modelled using two different models. These include the Suzen & Huang model, which solves for the electric field and charge density fields in order to obtain the body force, and the Greenblatt model, which simply assumes that the body force decays exponentially both downstream and normal to the actuator.

Keywords: Noise control, Landing gear, Tandem cylinders, Plasma actuation
I-INCE Classification of Subject Number: 30

1. INTRODUCTION

The number of passengers boarded in aircraft is predicted to be more than 7 billion by 2035 [1]. This indicates an increase of the air traffic, thus expansion of aircraft operations at airports. People living in proximity to airports are subject to high noise exposure, which adversely affect their health and wellbeing [2]. Major aircraft noise sources are located at the engine and airframe. Engine noise has been considerably reduced due to well optimized high bypass ratio turbo fan engines [3]. Airframe noise originates mainly from high lift devices and landing gears.

---

[1]wasala@chalmers.se
[2]leo.gonzalez@upm.es

Landing gear (LG) noise is more significant during the take-off or landing manoeuvres, therefore, has significant impacts to people living in the vicinity of airports. Landing gear noise is higher on large aircrafts such as A380 compared to other airframe noise sources, and reduces as the aircraft become smaller [4]. Mechanism of the landing gear noise is due to bluff body flow phenomena such as boundary layer separation, shear-layer instabilities and its impact on LG components, as well as extensive vortex motions.

A simplified landing gear geometry can lead to better understanding of the aerodynamic characteristics and consequently of noise generation mechanisms. In the present work, a tandem cylinder configuration has been chosen to mimic the effects of a landing gear, which consists of two cylinders placed with a separation in the stream-wise direction. Incoming flow interacts with the upstream cylinder and sheds into large vortex structures, which then impinge on the downstream cylinder [5]. There have been various studies with the change of the diameter (D) [6, 7], and with the change of the distance (L) between two cylinders [5, 8]. Zdravkovich's [9] work showed that the gap plays an important role and has effects on the flow characteristics. Cylinders do not behave as a single bluff body at subcritical Reynolds numbers when the gap is $3.2 < L/D < 3.8$. The flow behind the first cylinder switches between intermittent vortex shedding and constant vortex shedding, meanwhile constant vortex shedding occurs behind the second cylinder. Coherent structures, produced by the cylinders at this gap distance, have been observed in the tests by Jenkins et al. [10] and the numerical simulations by Lockard et al. [11] under the NASA framework of the Benchmark for Airframe Noise Commutations (BANC).

Dielectric Barrier Discharge (DBD) Plasma actuators have shown promising use for the aerodynamic flow separation control, which also have potential applications to aerodynamic noise control. A DBD plasma actuator consists of an exposed electrode and encapsulated electrode that are separated by a dielectric material (Figure 1). At high voltages, the air particles closer to the electrodes become weakly ionised (plasma) [12]. The electric field, which is generated by electrodes, acts on plasma and induces a body force field on the flow. This body force field can be manipulated for the flow separation control of tandem cylinder configurations.

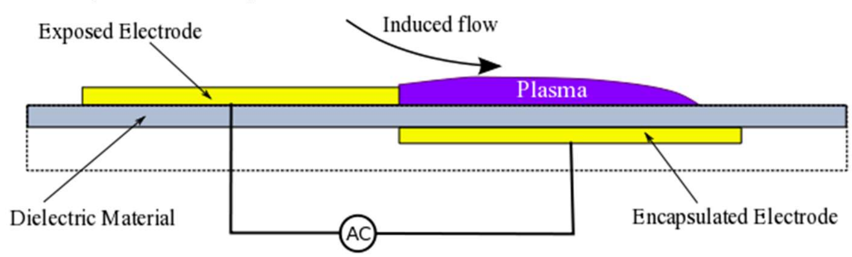

Figure 1: Schematic of a DBD plasma actuator

The effects of DBD plasma actuators have previously been modelled using simple electrostatic models and linearised force models. Models developed by Suzen & Huang (S-H) [12] and Orlov & Corke (O-C) [13] are examples of electro static models. In the S-H model, the electric field due to the electrodes and charged density fields are calculated separately. The electric field is solved using the Poisson equation. The charge density field is solved using a simple model, where the charge density at the wall is assumed to have a Gaussian distribution. This distribution function is voltage independent therefore this could lead to erroneous body force distribution. However, the model is simple to use and has been widely tested. Orlov & Corke developed a relatively detailed plasma model where actuators are modelled as a network of air capacitors, dielectric capacitors, plasma resistive elements and diodes in an electric circuit. Unlike the S-H model, the O-C model is time dependent. However, the model coefficients, which are frequency and voltage dependent, are empirically determined, therefore valid only for the given frequency and voltage.

Models developed by Shyy et al. [14] and Greenblatt et al. [15] are linearized body force models for prediction of the effects of plasma. In the Shyy model, simple electric field lines are generated that are approximately parallel to each other. This eliminates the need to calculate a detailed electric field. The model also assumes that the electric field decay linearly in space and ignore the effects of having more than one plasma actuators. This may lead to unrealistic body force fields. The Greenblatt model is a simple but satisfactory heuristic DBD plasma body-force model. The plasma actuation is represented by a volumetric force that is given by an analytic expression. Although the model is able to capture the essence of the flow control, inability to calculate wall normal body force is identified as a weakness.

Numerical investigation of plasma actuated flow on a tandem cylinders configuration, by Eltaweel et al. [16], shows noise reduction, at $Re_D = 22000$, with a single barrier discharge (SDBD) plasma actuator. Their semi-empirical plasma actuation model show good agreement with experimental aerodynamics and aeroacoustic data. The plasma actuation has been able to suppress the vortex shedding from the upstream cylinder, obtaining a noise reduction, at the downstream receiver locations, of 16 dB when the Mach number of the free-stream flow is 0.2.

The present work is a collaborative effort undertaken between Chalmers University of Technology and Technical University of Madrid (UPM) in the EU H2020 project IMAGE, focusing on a comprehensive exploration of flow induced noise generation mechanisms from the tandem-cylinders setup that mimic a landing gear configuration. Furthermore, the application of simple statistic plasma induced body force models is investigated for a possible noise reduction from the tandem cylinders configuration.

2. METHODOLOGY

1.1 Computational setup for hybrid RANS/LES modelling

The configuration adopted in CFD/CAA analysis is based on the experimental setup defined in the IMAGE project. The freestream velocity, U_∞ = 64 m/s. The atmosphere pressure is 101325 Pa and the temperature is 25°C. The dry air density is 1.225 kg/m^3. The heat capacity ratio is 1.4. The Reynolds number, Re, defined in terms of the diameter, D, of the cylinders and the freestream flow speed, is $Re_D = 1.75\times10^5$. The geometry of the tandem cylinder configuration, as shown in the Figure 1, is similar to the work by Lockard [11]. The diameter of cylinders defined in the IMAGE project is D = 0.04 m. The gap between the two cylinders is 3.7D. Two separate computational domains have been used for CFD simulations with two different meshes, generated by Chalmers and UPM, respectively.

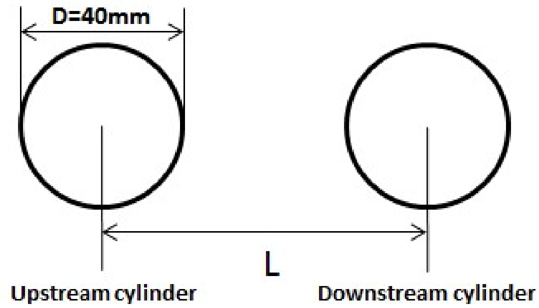

Figure 2: The tandem cylinders configuration

The computational work by Chalmers is based on a rectangular domain with a structured mesh generated using ANSYS ICEM CFD. The domain, as shown in Figure 3, is enclosed with a far-field boundary with a freestream Mach number of $M_\infty = 0.188$. Periodic conditions are imposed on the spanwise boundaries, no-slip wall boundary conditions on the cylinder surface and, moreover, the integral surface is taken as transparent boundaries to collect acoustic source data for predicting far-filed noise level using the Ffowcs Williams and Hawkings (FW-H) equation. Additionally, an acoustic suppression zone is added in the far field in order to damp out pressure waves and minimise acoustic reflections at the freestream boundary. The size of the domain is 45D×30D×3D in the streamwise, vertical and spanwise directions, respectively, yielding a 3.3% blockage (Figure 3a). The mesh, as shown in Figure 4, has 280 grid points along the circumference of the cylinder, and 90 grid points with uniform spacing in the spanwise direction. The y^+ is below unity. The mesh growth ratio is less than 1.05 in order to avoid any spurious acoustic reflections. The total number of cells is approximately 35 million on the mesh that was chosen after a mesh independent study.

The computational domain used by UPM is a cylinder of 42D and a span extent of 3D (Figure 3b). The mesh includes 5 blocks that allow to control the mesh size inside them independently. The refinement process is controlled by one single parameter called base size. A fully unstructured mesh was made using the STARCCM+ mesh generator. A static prism layer of 20 sublayers was included at each cylinder in order to keep $y^+<1$ along the cylinder perimeter. The number of cells in the selected mesh after the mesh convergence process is 20 million cells. The boundary conditions used are freestream for all the cylinder perimeter, periodic boundary conditions for the side boundaries and no slip conditions for both cylinders. Integral surfaces for the FW-H are aligned with the cylinder walls.

It has been assumed that the flow is fully turbulent in all the simulations, therefore no tripping device was included. The Hybrid RANS/LES simulations were conducted using the SST k-ω based IDDES method [17] for modelling turbulent flow physics with a second order upwind in the near wall RANS region blended with a second-order central scheme for LES in the off-wall region. Gradient computation is based on the hybrid Gauss-Least square method, where the gradient is determined using blended Green Gauss method and least square methods. An implicit second-order Euler backward scheme has been used for temporal discretisation.

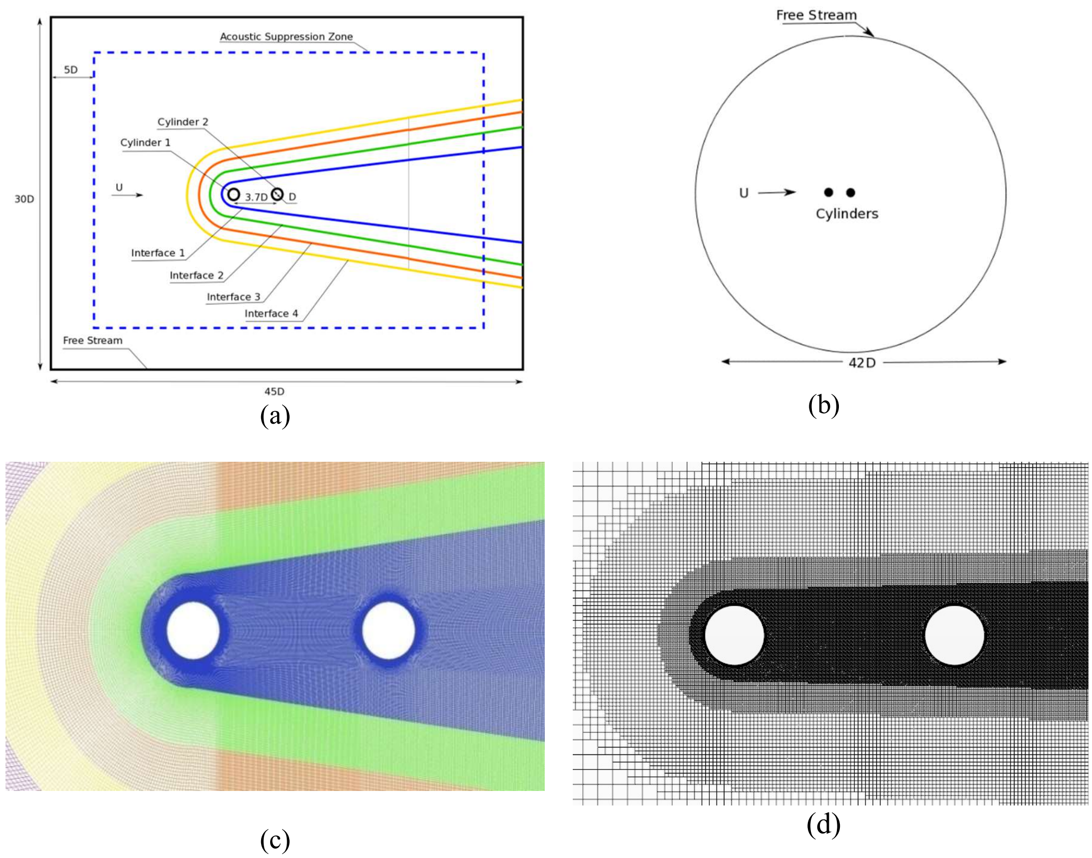

Figure 3: (a) and (b), Computational domain used in CFD simulations for the tandem-cylinders flow by Chalmers (a) and by UPM (b). (c) and (d) Computational mesh around the cylinders by Chalmers (c) and by UPM (d), respectively.

2.2 DBD plasma models and boundary conditions

The Suzen-Huang model

The Suzen-Huang (S-H) model was implemented by Chalmers in a 2D domain, where the electric field was solved using the electrostatic solver in STARCCM+. The charge density field was solved separately, based on the work by Suzen et al. [12]. Here, the surface charge density is defined as a Gaussian function, where the maximum value is located at the top of the coated electrode, closer to the exposed electrode. The function was calibrated using the maximum charge density field values given in the work by Brauner et al. [18]. The body force field was then calculated using the resultant electric field and charge density field. These forces were then added as a constant source term to the momentum equations. Therefore, it is assumed that the frequency of the plasma field have no effects on the flow. This is reasonable for the fact that the electrodes were charged with a high voltage and a very high frequency (20 kHz). An initial CFD stagnant simulation was conducted on a flat plate to verify the model with experimental results by Benard et al. [19] as shown in Figure 4.

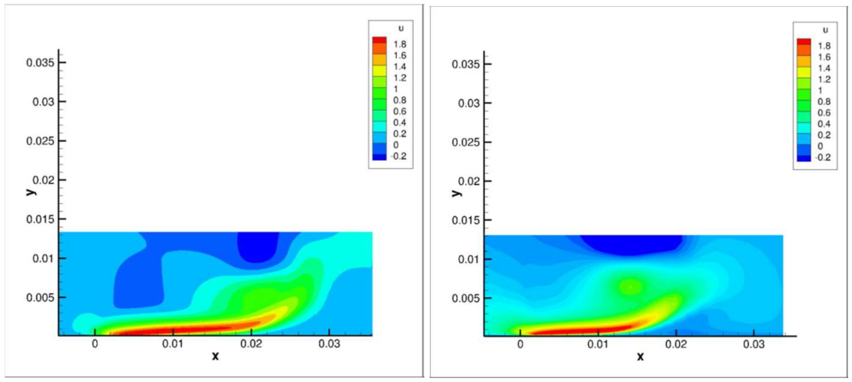

Figure 4. Contours of ionized air flow velocities with no external flow. Left: Experimental data for the U velocity measured using PIV [17]. Right: simulation results using the Suzen and Huang model [12].

The validated 2D flat plate model was then implemented in a 2D cylindrical geometry, see Figure 5, where two separate plasma actuators are implemented at 90° and 270°. The angle is defined clock-wise with respect to the stagnation point on the windward side of the cylinder. Finally, the 2D body force field was distributed to the 3D tandem-cylinder domain by assuming a uniform and constant body force along the spanwise direction.

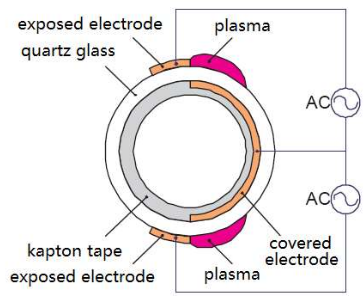

Figure 5: Schematic of a cylinder with a spanwise oriented DBD plasma actuator [16].

The Greenblatt model

The Greenblatt model was directly implemented in the tandem cylinder domain by UPM using built in user-defined functions in STARCCM+. The model was calibrated based on the maximum body force value of the S-H model. Comparison of the body force fields of the two models is shown in Figure 6. Here, both the models show the maximum body force at 90° location and decay towards the downstream direction. Greenblatt model predicts a relatively thick layer of plasma activity compared to the S-H model. Additionally, the Greenblatt model considers only tangential body forces, whereas the S-H model take in to account both tangential and wall normal body force vectors. The work by Bruner et al. [18] emphasised the importance of including the wall normal body force component, in the phenomenological S-H model, for a realistic reproduction of the effects of the DBD plasma actuator.

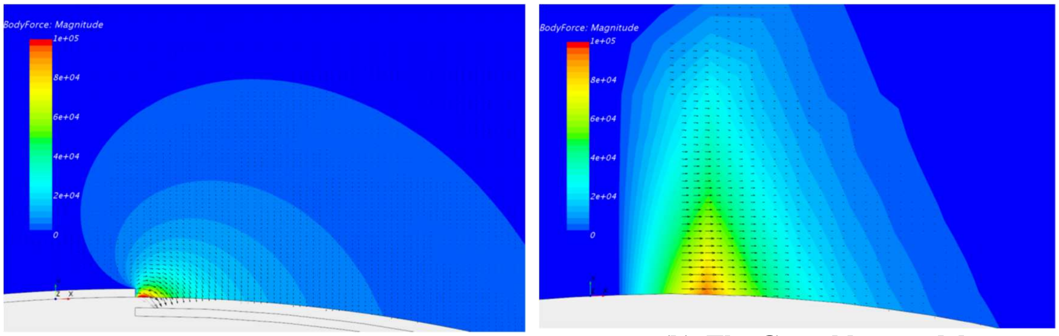

(a) The S-H model **(b) The Greenblatt model**

Figure 6: Body force magnitude estimated by the S-H model (Chalmers) and by the Greenblatt model (UPM).

3. RESULTS AND DISCUSSION

3.1 Aerodynamic results

Aerodynamic Force

CFD simulations have run for 0.4 second, where the final 0.2 s was used for time-averaged statistics and collecting acoustic source data. A time period of 0.2 s corresponds approximately to 144 vortex shedding periods of von Karman type behind the downstream cylinder. Figure 7 shows the oscillations of lift and drag coefficients of the downstream cylinder over a time duration of 0.265 – 0.295 second. Here, the fluctuation in lift shows approximately 6 times higher in magnitude compared to the fluctuation in drag. A single cycle of C_L oscillations covers two cycles of C_D oscillations. This is further analysed in Figure 8 (a) using the power spectra density (PSD) of C_L and C_D fluctuations, where the frequency of C_D (0.28) is twice that of C_L (0.56) in good agreement with the work by Bishop et al. [20]. In Figure 8, the *x*-axis indicates the Strouhal number, St $= f\ U_\infty/D$, the frequency normalised with $U_\infty = 64$ m/s and $D = 0.04$ m.

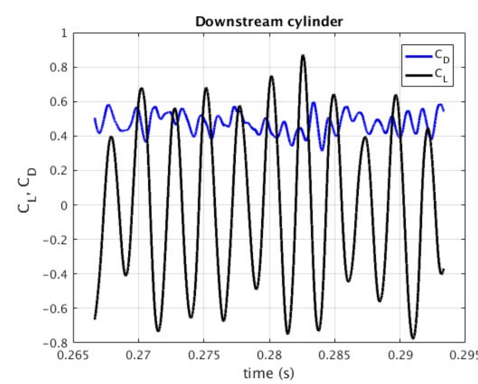

Figure 7: Instantaneous lift and drag coefficients of the downstream cylinder.

Figure 8 (b) shows the pressure spectral density at the stagnation point, θ = 0°, and on the top, θ =90°, of the downstream (the second) cylinder, respectively. The frequency at each tonal peak present in the PSDs shows good agreement with each other. This suggests further that the oscillations in aerodynamic forces are closely associated to the surface pressure fluctuations. More specifically, the oscillation in lift is impacted by the pressure fluctuations at the top of the cylinder, whereas the drag oscillation is directly connected to the pressure oscillation of the windward side of the cylinder. Therefore, the fluctuations in the aerodynamic forces may give evidence of the dipole acoustic sources in relation to the far field noise level, which will be further analysed using far field acoustic spectra. The tonal peaks in the PSDs of aerodynamic force and the surface pressure fluctuations indicate a shift of frequency to a high value, when the plasma effects are activated using the S-H model. However, this is not shown with Greenblatt model.

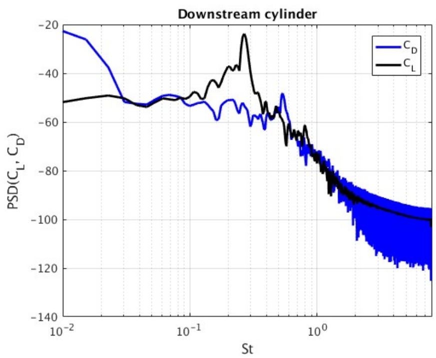

(a)

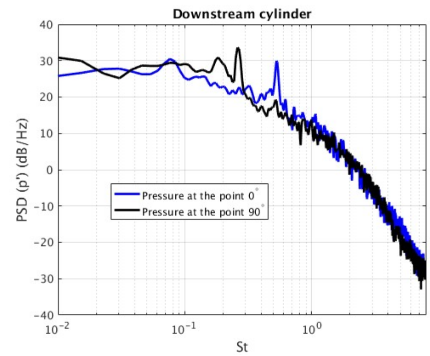

(b)

Figure 8: Power spectra of the lift and drag coefficient (a), power spectra of the pressure at locations *0°* and *90°* of the downstream cylinder (b).

Mean flow characteristics

Figure 9 shows the mean flow streamlines behind the upstream (the first) cylinder, with and without being subjected to the manipulation of the modelled plasma forces. When the S-H plasma model is activated at the first cylinder, the separation bubble becomes noticeably contained, and a secondary counter-recirculating separation bubble appears attached to the cylinder surface. The flow separation location on the first cylinder, estimated using time-averaged skin friction values, is delayed about 3°, from 94.7° to 97.5°, in the presence of the plasma force. The observation implies that the modelled body force has indeed energized the momentum in the wall layer, which has consequently delayed the boundary layer separation and induced further the secondary separation bubble. The Greenblatt model does not show a noticeable change in the separation bubble, however, the flow separation location was slightly delayed from 93.5° to 94.2°.

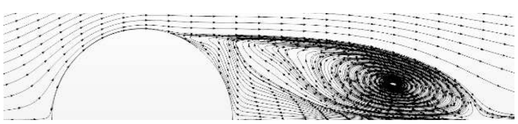

(a) No plasma- Structured mesh

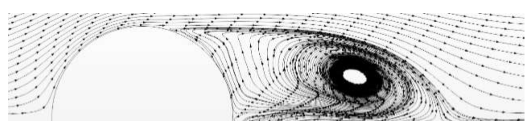

(b) No plasma – Unstructured mesh

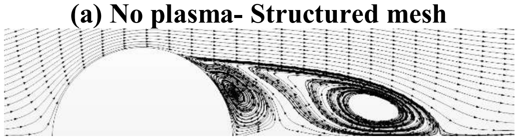

(c) Plasma on structured mesh- S-H model

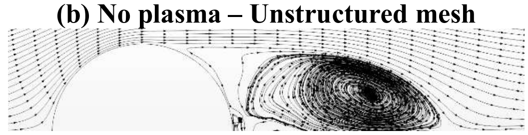

(d) Plasma on unstructured mesh- Greenblatt model

Figure 9: Mean flow streamlines with and without the effects of the DBD plasma actuator for the upstream first cylinder. (a, c) Chalmers, (b, d) UPM.

Figure 10 shows the time-averaged streamwise velocity along the centreline (*y/D = 0*) between the cylinders over the separation gap (Gap) and downstream of the second cylinder (Aft). The baseline computation by UPM using the unstructured mesh shows good agreement with the NASA experimental data [11]. It is noted here that the cylinder diameter and flow velocity defined in the IMAGE project is different compared to NASA experimental settings. The relatively large recirculation regions after the first and the second cylinder are shown in Figure 10 (a), as being predicted in the Chalmers computations on a structured mesh. For the baseline case (with no DBD plasma actuator), the IDDES on structured mesh has claimed a more extended separation bubble in the streamwise direction, compared to the computation using an unstructured mesh (UPM). The reversed flow in the separation bubble along the centreline is more intensive for X/D > 1.27 and becomes much alleviated when approaching the cylinder surface for x/D < 1.27. This has also been observed by Weinmann et al. [21] in their simulations using a structured mesh. With the plasma actuation, S-H model results, implemented using a structured mesh, have pronounced a much sensible response, for which the flow velocity along the centreline after the contained separation bubble is considerably increased. However, the Greenblatt model, implemented using an unstructured mesh, does not show a significant change in the velocity. Mean streamwise velocity values along the centreline in the wake of the downstream second cylinder suggests that the DBD actuation on the flow over the first cylinder has induced a slightly more extended separation bubble after the second cylinder. In the computation using a structured mesh, the streamwise velocity downstream the separation bubble after the second cylinder (for x/D > 5.5D) shows a faster growth along the centreline than in the baseline case, unlike the prediction given using the unstructured mesh that becomes very similar to the baseline flow.

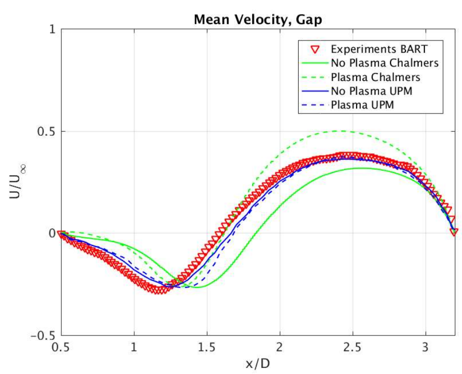

(a)

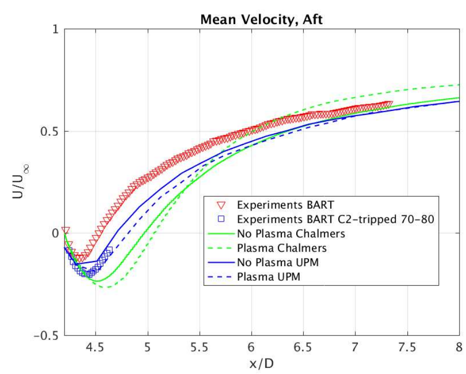

(b)

Figure 10: Mean streamwise velocity along the centreline between the two cylinders (gap) and downstream of the second cylinder (aft).

Figure 11 shows the IDDES-resolved instantaneous spanwise vorticity with and without DBD plasma actuation. Modelled with the S-H body force, the DBD plasma actuator has manipulated noticeably the free shear layer detached from the surface of the first cylinder, with the wake region relatively contained. This is consistent with the reduced size of the separation bubble as shown in Figure 9.

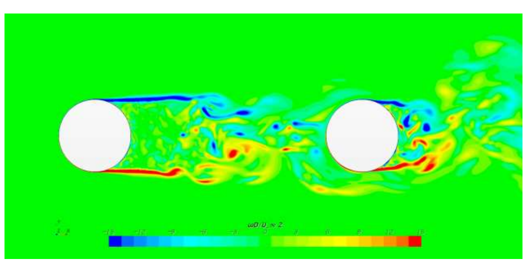

(a) No plasma

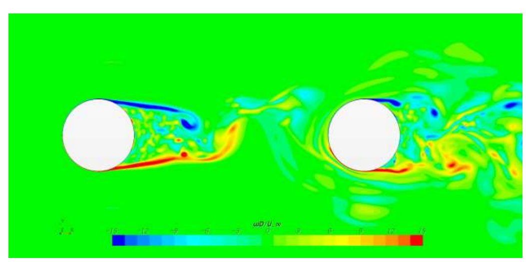

(b) Plasma modelled with S-H model

Figure 11: Instantaneous span-wise vorticity with and without plasma actuation.

Surface pressure characteristics

Figure 12 shows the coefficient of time-averaged surface pressure, C_p, and the coefficient of surface pressure fluctuations, C_{Prms}, on the downstream cylinder. The baseline simulation predictions, using different meshes, agree reasonably well with the experimental data. When the S-H plasma model is applied for the controlled case, the pressure at the stagnation point of the downstream cylinder noticeably increases, while the pressure at the top, bottom and behind the cylinder decreases. This is due to the effect of the plasma actuator. Without the actuators, the vortex structures that are generated from the free shear layer of the first cylinder reaches the front side of the downstream cylinder (Figure 11). With the DBD plasma actuators, the shear layer becomes more deflected towards the centreline, and the vortex motions in the downstream wake becomes less intensive. This suggests the interaction of vortex motions originated in the wake after the first cylinder with the second cylinder is somewhat mitigated and leading to increased surface pressure on the second cylinder. The computation using the unstructured mesh with the Greenblatt plasma model does not show any significant change. The pressure fluctuations in the both computational meshes, using respectively the S-H model and the Greenblatt model, show similar trends, where C_{Prms} decrease in relation to the plasma actuation. The S-H model shows relatively higher reduction of C_{Prms}. Surface pressure fluctuations are also acoustic dipole sources. It is thus anticipated that a reduction in C_{Prms} may lead to noise reduction.

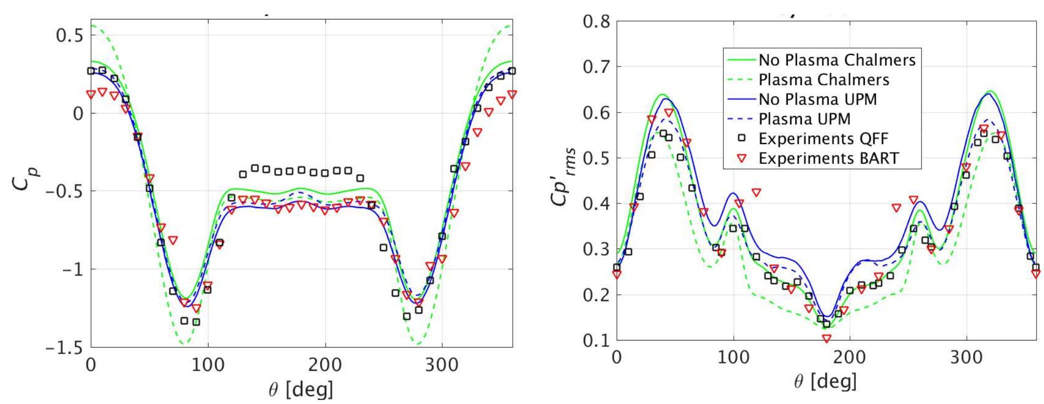

Figure 12: Time averaged surface C_p and C_{Prms} on the downstream cylinder.

3.2 Far-field aeroacoustic analysis

Figure 13 shows the acoustic pressure spectra taken at a far-field receiver located at 45D directly above the centre of the first cylinder. The acoustic spectra for the baseline case, computed using both meshes agree reasonably well with the measured data based on the NASA experimental setup. The predictions, using an unstructured mesh and FW-H integral surfaces that are aligned with the cylinder surface, by UPM shows better agreement in comparison to the predictions by Chalmers, particularly the main noise peak. The tonal noise takes place at St = 0.231 as measured by the experiment, while St = 0.225 in the unstructured mesh and St = 0.259 in the structured. It should be noted that the relatively high SPL peak predicted in the IDDES simulation using a structured mesh agrees well with the results by Weinmann et al. [21]. The main peak frequency corresponds to the vortex shedding frequency and in consistency to the frequencies for the C_L spectral peak and surface pressure spectral peak at $\theta = 90°$ of the downstream cylinder. There exists a secondary peak in the experimental spectrum at about St = 0.463

that is not predicted in computations. However, the third spectral peak at St = 0.698 is somewhat reflected in predictions.

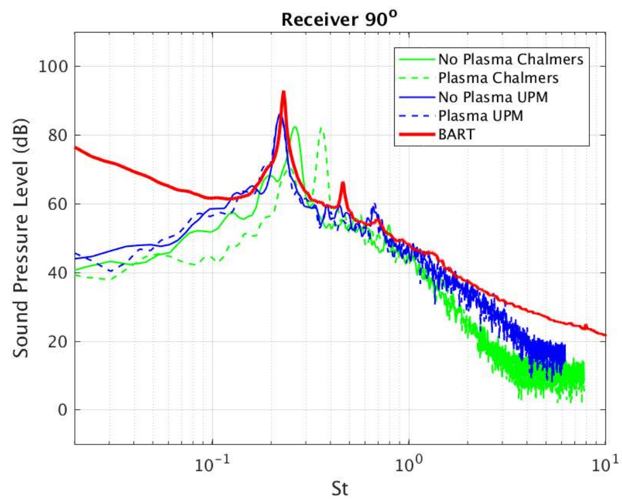

Figure 13: Acoustic spectra at the receiver located top far field relative to the centre of the upstream cylinder.

When the DBD plasma actuators are imposed, the S-H model has given rise of a shift of the tonal peak from St = 0.259 to St = 0.359. The major reduction in the SPL happens at lower frequencies for St < 0.359, while the high frequency noise does not show any significant difference. The noise level of the first tonal peak is reduced approximately 0.2 dB, which does not lead to any significant reduction in the overall sound pressure level. The Greenblatt model on the other hand does not show any shift in the frequency peak. The reason could be that the IDDES computation, with tangential body force vectors in the Greenblatt model, has only marginally manipulated shear layer and associated vortex shedding.

4. CONCLUDING REMARKS

The tandem-cylinders flow has been commutated using scale-resolving simulations based on the IDDES method using a structured and unstructured mesh, respectively. The baseline simulation using an unstructured mesh has produced predications closer to the experimental measurements, that is at the same Reynolds number, compared to the simulation using a structured mesh. This will be further verified when the experimental data from the IMAGE project is available.

The focus of the present work has been placed on the effect of the DBD plasma modelling on the flow and noise control. The S-H model and the Greenblatt models have been applied respectively to represent the effect of the DBD plasma actuator installed on the first cylinder. The S-H model consists of total body force vector, while the Greenblatt model includes only the tangential body force. The analysis shows that the S-H model has sensibly reduced the size of the separation bubble behind the first cylinder, leading to a narrowed wake region. This has consequently increased the vortex shedding frequency. The Greenblatt model does not trigger any significant changes of the free shear layer and associated acoustic features. This suggests that, represented with a body force, the impact of DBD plasma modelling may become significant and the direction of the body force must be carefully verified. In view of the ionized airflow properties by a DBD plasma actuator installed on a curvature surface, it seems that the normal body force component should not to be neglected for a realistic modelling of the effect of actuation.

5. ACKNOWLEDGEMENTS

This work was partially supported by the IMAGE project. IMAGE (Innovative Methodologies and technologies for reducing Aircraft Noise Generation and Emission) is an EU H2020 project by the European team (Chalmers, CFDB, CIMNE, KTH, NLR, NUMECA, RWTH-Aachen, ONERA, UPM, VKI, UPM, TU-K and AGI) in collaboration with the Chinese team (ASRI, BUAA, THU, NPU, IMech, BASTRI, ARI, FAI and ACAE). The project is funded by the EC in the H2020 Programme, under Contract No. 688971-IMAGE-H2020-MG-2014-2015. The simulations were performed on resources at Chalmers Centre for Computational Science and Engineering (C3SE) provided by the Swedish National Infrastructure for Computing (SNIC).

6. REFERENCES

1. Rius Vidales, A. F., Kotsonis, M., Alexandre, P. Antunes, A. P., and Cosin, R., *"Effect of Two-Dimensional Surface Irregularities on Swept Wing Transition: Forward Facing Steps."* AIAAConference (2018)
2. LeVine, M. J., Bernardo, J. E., Kirby, M., and Mavris, D. N., *"Placement of Runways at Capacity Constrained Airports to Minimize Population Exposure to Noise."* AIAA Conference (2018)
3. Leylekian, L., Lebrun, M., and Lempereur, P., *"An overview of aircraft noise reduction technologies." AerospaceLab* 6 (2014)
4. Huff, Dennis L., *"Noise reduction technologies for turbofan engines."* NASA/TM-2007-214495 (2007).
5. Zdravkovich, M. M., *"Review of flow interference between two circular cylinders in various arrangements."* Journal of Fluids Engineering (1977)
6. Alam, M. M., and Zhou, Y., *"Strouhal numbers, forces and flow structures around two tandem cylinders of different diameters."* Journal of Fluids and Structures (2008)
7. Novak, J., *"Strouhal number of two cylinders of different diameter arranged in tandem."* Acta Technica (1975)
8. Meneghini, J. R., Saltara, F., Siqueira, C. L. R., and Ferrari Jr., J. A., *"Numerical simulation of flow interference between two circular cylinders in tandem and side-by-side arrangements."* Journal of fluids and structures (2001)
9. Jenkins, L., Neuhart, D., McGinley, C., Khorrami, M., and Choudhari, M.,*"Characterization of unsteady flow structures around tandem cylinders for component interaction studies in airframe noise."* 11th AIAA/CEAS Aeroacoustics Conference. (2005)
10. Zdravkovich, M. M., *"Flow induced oscillations of two interfering circular cylinders."* Journal of Sound and Vibration (1985)
11. Lockard, D., Khorrami, M., Choudhari, M., Hutcheson, F., Brooks, T., and Stead, D., *"Tandem cylinder noise predictions."* AIAA/CEAS Conference (2007)
12. Suzen, Y., Huang, G., Jacob, J., and Ashpis, D., *"Numerical simulations of plasma based flow control applications*." In 35th AIAA Fluid Dynamics Conference and Exhibit (2005)
13. Orlov, D., Corke, T., and Patel, M., *"Electric circuit model for aerodynamic plasma actuator."* 44th AIAA Aerospace Sciences Meeting and Exhibit. (2006)
14. Shyy, W., Jayaraman, B., and Andersson, A., *"Modeling of glow discharge-induced fluid dynamics."* Journal of applied physics (2002)
15. Greenblatt, D., Schneider, S., and Schüle, C. Y., *"Mechanism of flow separation control using plasma actuation."* Physics of Fluids (2012)

16. Eltaweel, A., Wang, M., Kim, D., Thomas, F. O., & Kozlov, A. V., Numerical investigation of tandem-cylinder noise reduction using plasma-based flow control. *Journal of Fluid Mechanics*, (2014)
17. Gritskevich, M.S., Garbaruk, A.V., Schütze, J. and Menter, F.R., *"Development of DDES and IDDES formulations for the k-ω shear stress transport model"*. Flow, turbulence and combustion (2012)
18. Brauner, T., Laizet, S., Benard, N., and Moreau, E.,*"Modelling of dielectric barrier discharge plasma actuators for direct numerical simulations."* 8th AIAA Flow Control Conference (2016)
19. Benard, N., Caron, M., and Moreau, E., *"Evaluation of the time-resolved EHD force produced by a plasma actuator by particle image velocimetry-a parametric study."* Journal of Physics: Conference Series (2015)
20. Bishop, R. E. D., and Hassan, A. Y., *"The lift and drag forces on a circular cylinder oscillating in a flowing fluid."*Proc. R. Soc. Lond. A (1964)
21. Weinmann, M., Sandberg R. D., and Doolan, C., *"Tandem cylinder flow and noise predictions using a hybrid RANS/LES approach."* International Journal of Heat and Fluid Flow (2014)